This article was published in Chemical Engineering Journal, 253, 217-228, 2014
http://dx.doi.org/10.1016/j.cej.2014.05.037

Process enhancement at near neutral pH of a homogeneous photo-Fenton reaction using ferricarboxylate complexes: Application to oxytetracycline degradation

João H.O.S. Pereira [a], Daniel B. Queirós [b], Ana C. Reis [c], Olga C. Nunes [c], Maria T. Borges [b],

Rui A.R. Boaventura [a], Vítor J.P. Vilar [a,⇑]

[a] *LSRE – Laboratory of Separation and Reaction Engineering – Associate Laboratory LSRE/LCM, Faculdade de Engenharia, Universidade do Porto, Rua Dr. Roberto Frias, 4200-465 Porto, Portugal*

[b] *CIMAR – Centre for Marine and Environmental Research, Departamento de Biologia, Faculdade de Ciências da Universidade do Porto, Rua Campo Alegre, 4169-007 Porto, Portugal*

[c] *LEPABE – Laboratory of Process Engineering, Environment, Biotechnology and Energy, Departamento de Engenharia Química, Faculdade de Engenharia da Universidade do Porto, Rua Dr. Roberto Frias, 4200-465 Porto, Portugal*

Abstract

This work demonstrates the application at near neutral pH of a photo-Fenton reaction mediated by ferri-carboxylates on the treatment of aqueous solutions containing the antibiotic Oxytetracycline (OTC) under solar irradiation. The formation of a Fe:OTC complex after Fe^{2+} oxidation to Fe^{3+}, in the presence of H_2O_2, showed the inconvenience of using the conventional $Fe^{2+}/H_2O_2/UV–Vis$ process at near neutral pH levels, as the complex is retained in the filter. To overcome this, a Fe^{3+}/Oxalate/UV–Vis or Fe^{3+}/Citrate/H_2O_2/ UV–Vis process was proposed. The higher tendency of Fe^{3+} to form complexes with carboxylates avoids the formation of Fe:OTC complexes and allows for proper OTC detection along reaction times. The photo- Fenton process itself is improved by the extension of the iron solubility to higher and more practical pH values, by the increase of the quantum yield of Fe^{2+} production and by presenting stronger radiation absorption at wavelengths up to 580 nm. In this way, process efficiency

was evaluated for different variables such as Fe^{3+} concentration, pH, temperature and irradiance, using a compound parabolic collector (CPC) photoreactor at lab-scale under simulated solar radiation. Reaction rates were compared in the presence of different inorganic anions and humic acids, and in two different real wastewater matrixes. Results obtained in a CPC pilot-scale plant under natural solar light, using an iron/oxalate molar ratio of 1:3 ($[Fe^{3+}]$=2 mg L^{-1}, the maximum allowable discharge limit imposed by Portuguese regulations), at an initial pH of 5.0, showed that the antibiotic is quickly removed from solution, with consequent loss of activity on *Escherichia coli* (DSM 1103). The original DOC was decreased by 51%, with a remaining high percentage of low-molecular-weight carboxylate anions, and the final pH is within the legal discharge limits.

1. Introduction

Antibiotics are a special group of pharmaceuticals used to control infection diseases in human and veterinary medicine. Residual concentration have been detected in various environmental compartments worldwide due to the fact that a large percentage of the consumed antibiotics are not completely metabolized (and thus are excreted as active substances) and that conventional wastewater treatment methods fail to completely remove them from solution [1–3]. Even though direct cause and effect relation- ships are still to be established, it is widely recognized that antibiotic pollution contributes to antibiotic resistance dissemination [4,5]. Thus, research in recent years has been focused on alternative ways to prevent the contamination of water supplies by this kind of pollutants. Urban wastewater treatment plants (WWTP) are one of its major sources [6], but highly-contaminated effluents resulting from fish farming activities may also be a special case to be considered [7].

Advanced oxidation processes (AOPs), a class of treatments involving different ways of generating the highly reactive and non-selective hydroxyl radical (·OH) and other reactive oxygen species [8], have been considered for the removal of these sub- stances, especially those involving catalysis and solar irradiation such as the photo-Fenton process [9,10]. Photo-Fenton comprises the combination of ferrous iron (Fe^{2+}) with hydrogen peroxide (H_2O_2) and (solar) UV–Vis radiation resulting in the production of two moles of ·OH per mole of hydrogen peroxide (Eqs. (1) and (2)), as simplified by Gogate and Pandit [8]:

$$Fe^{2+} + H_2O_2 \rightarrow Fe^{3+} + {\cdot}OH + HO^- \quad (1)$$

$$Fe(OH)^{2+} + h\upsilon \rightarrow Fe^{2+} + {\cdot}OH \quad (2)$$

Pignatello et al. [11] summarizes the reasons for the optimum operational pH value of the (photo-) Fenton process around 3 as follows: first, the solubility of Fe^{3+}–hydroxy complexes decreases for pH values above 3; second, $[Fe(OH)]^{2+}$, the most photoactive species (with absorption bands between 290 and 400 nm), reaches its maximum molar fraction around the aforementioned pH. As a consequence, there is a limited viability of applying this process in industrial scale due to the costs associated with pH corrections (initial acidification and final neutralization).

Antibiotics are also known to form stable complexes with metallic cations [12]. This cation:antibiotic interaction results in different physical properties which are environmentally relevant in many ways. Several works have reported, for instance, on the enhanced [13] or decreased [14] antibacterial properties, negative effects on soil microbial community [15] and on the sorption and mobility behaviour in soils and aquatic sediments [16,17]. Pertinent to the photo-Fenton process is the formation of complexes between antibiotics and Fe^{2+} and Fe^{3+} for two reasons. It not only decreases degradation efficiencies (due to a lower iron availability to react with hydrogen peroxide [18]), but it may also lead to mistaken readings in analytical equipments (e.g., different retention times in HPLC chromatograms and/or different UV absorption spectra [19]), thereby to incorrectly calculated reaction rates. However, this can be overcome by recurring to the complexation of Fe^{3+} with carboxylate ions, which also improves the photo-Fenton process by extending the solubility of iron to higher and more practical pH values, by presenting stronger radiation absorption at wavelengths until 580 nm and by increasing the quantum yield of Fe^{2+} production according to Eq. (3) [11,20]

$$Fe^{3+}(C_2O_4)_n^{(3-2n)} + h\upsilon \rightarrow Fe^{2+} + (n-1)C_2O_4^{2-} + C_2O_4^{2-\cdot} \quad (3)$$

Ferricarboxylate-mediated solar photo-Fenton has already been successfully applied to the treatment of different wastewaters and specific pollutants, whereby carboxylate ions such as oxalate, citrate and EDDS (ethylenediamine-N,N⍬-disuccinic acid) were used to form complexes with Fe^{3+} [21–23].

Considering the current limitations of implementing these processes in existing WWTP (high flow rates, capital and reactant costs, removal of excess iron to comply with discharge limits, for example), the combination of membrane

processes with AOPs have been recently proposed [24]. Miralles-Cuevas et al. [25], for instance, have shown that mild solar photo-Fenton is best applied to higher micropollutants loads found in nanofiltration concentrates (up to the mg L^{-1} range), thus minimizing their disposal impact.

In this context, the aim of this work was thus the process enhancement at near neutral pH conditions of a homogeneous solar photo-Fenton reaction through the use of ferricarboxylates complexes applied to the removal of Oxytetracycline in aqueous solutions. Experiments at lab-scale using a CPC photoreactor under simulated solar radiation were performed to (i) compare the conventional Fe^{2+}/H2O2/UV–Vis with the Fe^{3+}/Oxalate/UV–Vis or Fe^{3+}/Citrate/H2O2/UV–Vis systems, (ii) choose the optimum dis- solved Fe^{3+} concentration (iron/oxalate molar ratio of 1:3) and also (iii) the initial working pH level. The influence of temperature, irradiance, and the presence of humic acids and of some commonly occurring inorganic ions in several types of wastewaters was also assessed. Matrix effects were studied by spiking OTC in two different media, a WWTP effluent after secondary treatment and a real trout farm effluent. Experiments in a solar pilot-scale plant equipped with CPCs were also carried out to evaluate the performance of the reaction under natural solar radiation conditions, the abatement of OTC, antibacterial activity and the composition of the remaining dissolved organic carbon in terms of low- molecular-weight carboxylate ions.

2. Materials and methods

2.1. *Reagents*

Oxytetracycline hydrochloride was purchased from Sigma– Aldrich (>97% purity; MW = 496.89 g mol^{-1}; molecular structure, UV absorbance spectrum and speciation diagram as a function of pH shown in Fig. S1). Photo-Fenton experiments were performed using hydrogen peroxide (Quimitécnica, S.A., 50% (w/v), 1.10 g cm^{-3}), ferrous sulphate heptahydrate (Panreac), ferric chlo- ride hexahydrate (Merck), oxalic acid dihydrate (VWR Prolabo, purity P 98%) and citric acid monohydrate (VWR; 100%). Sulfuric acid (Pronalab, 96%, 1.84 g/cm^3) and sodium hydroxide (Merck) were used for pH adjustment. Humic acids were Alfa Aesar (CAS# 1415-93-6), whereas NaCl, MgSO4 7H2O, NaHCO3, KNO3, were all analytical grade. Ultrapure and deionized water necessary for analysis were produced by a Millipore® system (Direct-Q model) and a reverse osmosis system (Panice®), respectively. For HPLC, gra- dient-grade acetonitrile and methanol were obtained from Merck, while oxalic acid dehydrate (100%) was from VWR Prolabo.

2.2. *Photocatalytic apparatus*

2.2.1. *Lab-scale photoreactor*

The experiments performed to evaluate the efficiency of Fe^{2+}/H2O2/UV–Vis, Fe^{3+}/Oxalate/H2O2/UV–Vis and Fe^{3+}/Citrate/H2O2/UV–Vis processes on the degradation and mineralization of OTC were carried out in a lab-scale photoreactor provided with a sunlight simulator. A schematic representation and a detailed description can be consulted elsewhere [26].

2.2.2. *Solar Pilot plant*

The solar photocatalytic experiments were carried out in a CPC pilot plant installed at the roof of the Chemical Engineering Department of the Faculty of Engineering, University of Porto (FEUP), Portugal. A schematic representation and a detailed description of the pilot plant can also be consulted elsewhere [26]. The accumulated UV energy ($Q_{UV,n}$, kJ L^{-1}) was calculated according to Eq. S1 (Supplementary Data).

2.3. *Experimental procedure*

2.3.1. *Lab-scale photoreactor tests*

In all the experiments, a solution of 1.2 L of OTC (C_0 = 20 mg L^{-1} = 4.34x10^{-2} M), was added to the recirculation glass vessel and homogenized by stirring in darkness. The working OTC concentration of 20 mg L^{-1} has been chosen bearing in mind the available analytical equipment and also the possibility of applying the processes under study in the decontamination of concentrates resulting from membrane separation processes, or from effluents resulting from fish farm bath immersion treatments using high antibiotic concentrations, as mentioned above. The temperature of the thermostatic bath was controlled to keep the antibiotic solution at 25 ºC. After 15 min, a sample was taken to confirm the initial OTC and DOC concentrations (preliminary tests showed no absorption of OTC onto the glass vessel and borosilicate glass tubes). In the Fe^{2+}/H2O2/UV–Vis experiments, the initial pH was adjusted to 3.0, 4.0 or 5.0 with sulfuric acid and another sample was taken after 15 min. Ferrous sulfate was added in order to achieve a concentration of 2 mg L^{-1} Fe^{2+}. The solution was left to homogenize for 15 min, after which another sample was taken, and the initial iron concentration was also confirmed. The solution was then pumped to the CPC unit (illuminated volume (V_i) = 270 mL; V_i/V_t = 0.34; illuminated time (t_i) = 0.43 min;

dark time (t_{dark}) = 1.16 min; A_{CPC} = 0.025 m^2) before the SUNTEST was turned on. Irradiation was set as I = 500 W m^{-2}, which is equivalent to 44 W_{UV} m^{-2} measured in the wavelength range from 280 to 400 nm [26]. Immediately after irradiation began, the initial H_2O_2 dose was added, while the pH of the solution was left uncontrolled.

The same procedure was followed in the Fe^{3+}/Oxalate/H_2O_2/ UV–Vis and Fe^{3+}/Citrate/H_2O_2/UV–Vis experiments, except for the addition of a 1:3 iron/oxalate molar ratio dose (extra DOC~2.6 mg L^{-1}), or a 1:1 iron/citrate molar ratio dose (extra DOC~4.3 mg L^{-1}), before the pH adjustment and ferric chloride addition steps. When applied, the addition of inorganic ions ([Cl^-] = [SO^{2-}] = [NO^-] = 1 g L^{-1}; [HCO^-] = 0.1 g L^{-1}; values based on the inorganics concentration ratio of Miralles-Cuevas et al. [25]) and natural organic matter (humic acids, extra [DOC] ~5 mg L^{-1}, based on Lindsey and Tarr [27]) to the initial OTC solution was also carried out. Matrix effects were studied by spiking OTC in two different effluents, and compared to the analogous results obtained using deionized water (DW). Wastewater effluent (WW) was collected after secondary treatment in a urban WWTP (Northern Portugal), while trout farm effluent (TF) was collected in the outlet of a trout farm operated in open circuit regime (Northern Portugal), after final decantation. The main characteristics of the tested effluents are presented in Table 1.

The addition of H_2O_2 was based on the stoichiometric amount necessary to completely mineralize 20 mg L^{-1} of OTC, according to Eq. (4), which is 67 mg L^{-1} (2.3 mM) of H_2O_2.

$$C_{22}H_{24}N_2O_9 + 52H_2O_2 \rightarrow 22CO_2 + 63H_2O + 2HNO_3 \quad (4)$$

However, a control dosage strategy was followed in order to avoid excess H_2O_2 in solution, which would result in undesirable side reactions, including peroxide dismutation, producing an excess of reagent consumption [28,29]. In this way, an initial 30 mg L^{-1} dose (~0.9 mM) was added in the beginning of every experiment, and supplementary 30 mg L^{-1} additions were per- formed when the H_2O_2 concentration approached 10 mg L^{-1} (~0.3 mM) along the reactions to avoid stopping the reaction.

Samples were then taken during the experiments at predefined times and filtered through 0.45 μm Nylon VWR membrane filters before analysis to evaluate the photodegradation process. For HPLC analysis, samples were quenched with

methanol to stop any further reactions [30], while DOC determination was performed immediately without previous treatment. Dark Fenton effects were negligible.

2.3.2. *Solar pilot plant*

In the solar pilot plant, Fe^{3+}/Oxalate/H_2O_2/UV–Vis experiments were performed using the optimized parameters obtained at the lab-scale system, in order to evaluate the process performance under natural solar irradiation. The required OTC mass to obtain C_{OTC} = 20 mg L^{-1} was dissolved in 15 L of deionized water added to the recirculation tank of the CPC units (illuminated volume (V_i) = 5.1 L; V_i/V_t = 0.34; illuminated time (t_i) = 0.25 min; dark time (t_{dark}) = 0.50 min; A_{CPC} = 0.455 m^2), and homogenized by turbulent recirculation during 30 min in darkness. A first sample was taken to confirm OTC and DOC concentrations. Oxalic acid was added (iron/oxalate molar ratio of 1:3), left to recirculate for 15 min, and a second sample was taken before the addition of ferric chloride (2 mg Fe^{3+} L^{-1}) and pH adjustment to 5.0. A third sample was taken after 15 min, and the initial iron concentration was con- firmed. The CPCs were uncovered, the same initial H_2O_2 dose was added and the pH of the solution was left uncontrolled. Along the experiment, the average solution temperature was 26.1 ºC, while the average measured incident radiation was 16.2 W_{UV} m^{-2}. Samples were taken at pre-defined times to follow the photodegradation process and pre-filtrated through 0.45 µm Nylon VWR membrane filters before analysis.

2.4. *Analytical procedures*

A detailed description of the analysis of OTC concentration (HPLC-DAD), dissolved organic carbon (DOC) content (TC-TOC- TN analyzer), global UV radiation, UV absorbance spectra and low-molecular-weight carboxylate anions (LMWCA, ion chromatography) can be consulted elsewhere [31]. Additional LMWCA analysis was performed in the same HPLC-DAD system, using a Rezex™ ROA-Organic Acid H^+ (8%), LC Column 300 × 7.8 mm). The isocratic method used 0.005 N H_2SO_4 delivered at a flow rate of 0.5 mL min^{-1}. Run time was 50 min, injection volume 10 µL and the wavelength of the detector was set at 210 nm.

Concentration of H_2O_2 was measured by the metavanadate method, according to Nogueira et al. [32]. Dissolved iron concentration was determined by colorimetry with 1,10-phenantroline, according to ISO 6332.

Antimicrobial activity assays were carried out in 96-well micro- titer plates using

a Synergy HT Multi-Mode Microplate Reader (Biotek Instruments, USA), and *Escherichia coli* DSM 1103 as test strain. Samples collected over time were supplemented with 2 g L^{-1} of yeast extract and inoculated with the test strain at an initial optical density at 610 nm of 0.08. Cultures were grown at 30 ºC and 300 rpm for 20 h. Controls with different OTC concentrations (0–20 mg L^{-1}) were grown in parallel under the same conditions. Normalized biomass yield was obtained by dividing the biomass yield of the culture grown in the sample by the biomass yield obtained in the absence of OTC.

A pseudo-first-order mathematical model was fitted to the experimental data obtained from the kinetic studies by a non- linear regression method (software Fig.P for Windows from Fig.P Software Incorporated).

3. Results and discussion

3.1. *Conventional Fe^{2+}/H2O2/UV–Vis reaction*

In a previous work it was reported the effect of solar and simulated solar photolysis on OTC degradation [33], which can be expected from the relative overlapping of the UV absorbance spectrum of OTC with both solar and xenon lamp spectra, as seen in Fig. 1c. Pseudo-first order kinetics, for instance, was found to be one order of magnitude lower in the case of solar photolysis of OTC (0.205 ± 0.005 L kJ^{-1}) when compared to solar photocatalysis mediated by 0.5 g L^{-1} of TiO_2 (2.63 ± 0.03 L kJ^{-1}). Slow antibiotic degradation and lack of proper mineralization has brought up the need of exploring more effective oxidative methods.

The results of the conventional Fe^{2+}/H_2O_2/UV–Vis degradation of OTC under different initial pH values (3.0, 4.0 and 5.0), carried out in a lab-scale photoreactor equipped with a CPC, are shown in Fig. 2a. The concentration of Fe^{2+} was 2 mg L^{-1}, which is the total iron discharge limit into any water body, according to the Portuguese legislation (Decreto-Lei n.º236/98 [34]), while H_2O_2 concentration was kept between 10 and 30 mg L^{-1} (0.3 to 0.9 mM; total addition around 3.1 mM). In the three experiments per- formed, after the first addition of H_2O_2, the concentration of OTC approached LOQ levels approximately after 4 min of illumination (0.22 kJ_{UV} L^{-1}). DOC levels slowly decreased down to near 30% of their initial values by the end of the photo-treatment period (45 min, 2.7 kJ_{UV} L^{-1}), while an average of 1.5 mM of H_2O_2 was consumed. Overall similar results were obtained by Bautitz and Nogueira [35], who applied photo-Fenton mediated by ferric nitrate and potassium

ferrioxalate at pH = 2.5 under black-light and solar irradiation to study the degradation of Tetracycline. In the present study, the only differences between the three experiments performed lie in the behaviour of the solution pH and in total dissolved iron concentration in the pH0 = 5.0 experiment. According to the OTC speciation diagram (Fig. S1b), for pH values between 3.0 and 5.0, the molar fraction of zwitterionic OTC (H_2OTC) increases from 0.5 to nearly 1.0. Figueroa and Mackay [36] reported that the expected initial decrease in the concentrations of OTC and DOC with increasing pH after the iron salt addition step is a consequence of the interaction between ferrous hydrous oxides and deprotonated OTC species. Taking into consideration Eq. (1), after the Fe^{2+} oxidation step to Fe^{3+}, the rapid decay of the antibiotic may be explained by the formation of stable complexes between OTC and Fe^{3+}, which, according to the abovementioned authors, strongly interferes with HPLC measurements and may induce in erroneous kinetic calculations. Overall stability constants of the Fe^{2+}–OTC and Fe^{3+}–OTC complexes of 10.4 and 22.0, respectively, reported by Albert [37], support this conclusion. A survey of the available literature concerning Fe–OTC complex formation has shown a lack of agreement regarding the role of the different OTC species and the functional groups of the molecule in the stepwise formation of the 1:1, 1:2 and 1:3 metal-antibiotic complexes as a function of pH. Nevertheless, for clarification purposes, we have attempted to model the complex formation between OTC and Fe^{3+} using the equilibrium computer program MINEQL+ [38]. As it can be seen in Fig. S2a (left), a large fraction of Fe^{3+} is expected to form complexes with the antibiotic. Bench- scale tests confirmed that by increasing the pH from 3.0 towards 5.0 of solutions containing only 2 mg L^{-1} Fe^{3+} and 20 mg L^{-1} of OTC, the original concentration of OTC not only gradually decreases but it also differs from filtered and non-filtered samples (data not shown). The same phenomenon occurs with DOC. As such, the complete removal of OTC from solution by the conventional photo-Fenton reaction with increasing initial pH values could not be directly attributed. Zhou et al. [39] reported on the photo-reduction of Fe^{3+} in the Fe–OTC complex, which is expected given the broad range of its UV–Vis spectrum (Fig. S1c), leading to the oxidation of the OTC organic ligand. The low apparent quantum yield of the Fe^{3+}–Tetracycline complex photolysis, even at its highest UV absorbance peak (0.098, k = 254 nm, pH = 3), may add to the decrease in H_2O_2 decomposition by the Fenton reaction and in the overall efficiency of the photo-Fenton process.

Silva et al. [40] have demonstrated how the addition of organic ligands such as oxalate or citrate displace the herbicide tebuthiuron (TBH) from the non-photoactive Fe^{3+}–TBH complex, improving the degradation process of TBH via

the photo-Fenton reaction. In this way, we have introduced the oxalate and iron-oxalate equilibrium reactions in MINEQL+ in order to calculate the formation of complexes between 2 mg Fe^{3+} L^{-1} with both 20 mg L^{-1} OTC and 9.5 mg L^{-1} oxalate (1:3 iron/oxalate ratio) present in solution. Fig. S2a (right) shows that the added oxalate clearly competes with OTC for the available Fe^{3+} in the pH range of interest. In the presence of oxalate, the concentration of OTC can also be properly followed by HPLC-DAD, which allows for a proper kinetic study. Taking this and the objective of operating this process at neutral pH values, the ability of carboxylates to improve the photo-Fenton process was henceforth studied.

3.2. *Fe^{3+}/Carboxylate/H_2O_2/UV–Vis OTC degradation reactions*

3.2.1. *Influence of iron concentration*

Fig. 2 presents the OTC degradation efficiency by the photo- Fenton reaction using low iron concentrations in the threshold of the abovementioned iron discharge limit (1.0, 2.0 and 5.0 mg L^{-1}), with an iron/oxalate molar ratio of 1:3, without initial pH adjustment. The degradation profiles of OTC were very similar for all tested Fe^{3+} concentrations, and the calculated pseudo-first order kinetic rates are presented in Table 2. A clear increase of reaction rates occurs with increasing iron amounts, but even with the lowest concentration tested, 1 mg L^{-1}, OTC was no longer detected (LOD = 0.10 mg L^{-1}) after 10 min of reaction (0.6 kJ$_{UV}$ L^{-1}). By the end of the photo-treatment period (45 min, 2.75 kJ$_{UV}$ L^{-1}), 80% mineralization was achieved with both 2 and 5 mg L^{-1} of Fe^{3+}, although a higher H_2O_2 consumption occurred with the highest Fe^{3+} concentration. In contrast, for 1 mg L^{-1} of Fe^{3+} only ~50% mineralization was achieved, with less H_2O_2 consumed than for the other Fe^{3+} concentrations. A direct relationship between the increases in hydroxyl radical formation and the initial Fe dosage is expected according to Eq. (1). The avoidance of the need of an iron removal step at the end of the treatment, associated with a satisfying mineralization degree, has shown 2 mg L^{-1} to be the concentration that represented the working option for photo-Fen- ton treatment with Fe^{3+}–oxalate complex.

The pseudo-first order kinetic rate constant of the 2 mg Fe^{3+} L^{-1} experiment, 8.6 ± 0.5 L kJ^{-1}, was the double of the rate constant reported in our previous work regarding the solar photocatalytic degradation of OTC in the presence of 0.5 g L^{-1} TiO_2 at a neutral pH, carried out with the same experimental installation, 4.3 ± 0.4 L kJ^{-1} [31].

3.2.2. *Influence of initial solution pH*

After the previous experiments, the effect of the initial solution pH value was studied in order to find the highest possible working pH without compromising the reaction efficiency. The results, presented in Fig. 3, show that with unadjusted initial pH (4.1), pH = 5.0 and pH = 6.0, OTC was no longer detected after 5, 10 and 15 min of illumination time (0.3, 0.6 and 0.9 kJ L^{-1} of accumulated UV energy, respectively). By the same order, DOC concentration was reduced by 75%, 51% and 37% of its initial value after 45 min of reaction (2.78 kJ_{UV} L^{-1}). Despite the decreasing mineralization efficiency with increasing pH, there was not much difference between H_2O_2 consumption profiles.

First of all, it must be noted that after the oxalate and iron addition steps and consequent pH adjustment, the initial concentration of OTC still decreases with increasing pH. Examining the pH range between 4 and 6 in the attempted iron speciation diagram (Fig. S2a, right), the sum of the fractions of oxalate and OTC iron complexes remain somewhat constant, while the formation of an iron solid phase (Ferrihydrite, $Fe(OH)_3$ (s)) is expected to form and rapidly increase after pH 5. Given the variation in both $Fe(C_2O_4)^+$ and $Fe(C_2O_4)^{3-}$ fractions, as well as in 1:2 and 1:3 Fe–OTC complexes, the observed phenomenon could be attributed either to a diminishing strength in complexing iron by $Fe(C_2O_4)^{3-}$ in favor of the 1:3 Fe–OTC complex, or to the slow formation of amorphous $Fe(OH)_3$(s), confirmed by the lower initial dissolved iron concentration measured in the experiments at pH 5.0 and 6.0 (Fig. 3). As soon as irradiation started, a competition phenomenon between both ligands (oxalate and OTC) to form complexes with iron occurs, as seen by the erratic behaviour of DOC. A comparison with unfiltered DOC samples (data not shown) showed that in some sample points DOC is again retained in the filter. After hydroxyl radical attack to the original antibiotic molecule, some of the degradation products seems to retain Fe^{3+}-chelating properties, whereby being retained in the filter at higher pH levels. However, after very low OTC concentrations, more iron is able to be chelated by oxalate, since a small increase in total dissolved iron concentration is showed at 15 min. After this period, filtered and unfiltered DOC was found to be the same, so proper mineralization corresponds well with the marked increase in H_2O_2 consumption and possibly with the decarboxylation of ferrioxalate complexes, since iron levels begin to drop as well. Furthermore, to counter the lower amount of total dissolved iron along the pH = 6.0 trial, an extra dose of oxalic acid was added after this same point. Although indeed iron concentration increased, it quickly began to drop, with no considerable increase in the mineralization rate.

Regarding the influence of pH in the photochemistry itself, the role of the

speciation of the main Fe^{3+}–oxalate complexes must be underlined. Recently, Weller et al. [41] determined individual quantum yields for $Fe(C_2O_4)^{-}_2$ as 1.17 (366 nm) and 1.40 (436 nm), and for $Fe(C_2O_4)^{3-}$ as 0.91 (366 nm) and 1.00 (436 nm). A speciation diagram discarding the Fe–OTC species, previously included for expository purposes only, has been calculated in the same manner (Fig. S2b, left). Cumulatively, $Fe(C_2O_4)^{-}_2$ and $Fe(C_2O_4)^{3-}$ are the main iron species in the studied pH range, albeit with changing proportions over pH. The fraction of $Fe(C_2O_4)^{-}_2$ lowers smoothly from 0.7 down to less than 0.1, whereas the fraction of $Fe(C_2O_4)^{3-}$ evolves from near 0.3, to a maximum of approximately 0.5 at pH = 5.0, and finally gets to less than 0.1 at pH = 6.0. Hence, by pH = 6.0, total iron precipitation would be expected. However, this precipitation occurs slowly, and Fe^{3+} may not be in equilibrium with the solid phase [42], so some oxalate is still expected to be found in solution, which may help to explain the decrease in the initial dissolved iron concentration shown at the maximum pH level tested.

The decreasing reaction rates at pH 4.1, pH = 5.0 and pH = 6.0 experiments, 8.6 ± 0.5, 6.3 ± 0.2 and 2.3 ± 0.1 L^{-1} kJ, respectively, appear to reflect this relationship between the molar fractions of the referred iron–oxalate complexes and their respective quantum yields. On the other hand, the positive influence of increasing solution pH on OTC degradation by means of its solar/visible light absorption properties, as described by Zhao et al. [43], did not seem to play a significant role in this process.

Considering these results, the working pH of 5.0 was chosen for the subsequent set of experiments, since no extra dosage of oxalic acid was needed to obtain a satisfactory 49% mineralization of the initial DOC content, OTC was no longer detected after 10 min of illumination time (Q_{UV} = 0.6 kJ L^{-1}), and the final pH value of the solution approached the legal lower discharge pH value of 6.0 (Decreto-Lei no. 236/98).

Before proceeding, two more experiments were performed: Fe^{3+}/Citrate/H_2O_2/UV–Vis system with 2 mg L^{-1} of Fe^{3+} and 1:1 iron/citrate molar ratio to compare the results with the previous unadjusted and adjusted initial pH = 5.0 Fe^{3+}/Oxalate/H_2O_2/UV– Vis reactions. It can be seen in Fig. 4 that for both initial pH values, the concentration of OTC after the citrate and ferric iron addition steps sharply decreases after only a minute of illumination time (Q_{UV} = 0.07 kJ L^{-1}). The residual amount (12% of $[OTC]_0$ in both cases) is slowly degraded until OTC is no longer detected after 5.0 and 7.5 min of reaction (0.3 and 0.4 kJ_{UV} L^{-1}) for unadjusted pH_0 and controlled pH_0 = 5.0, respectively. In the same order, the

respective DOC content was reduced to 31% and 54% of its initial value by the end of the illumination periods, while an average of 1.49 mM of H_2O_2 was consumed. The Fe^{3+}/Citrate/H_2O_2/UV–Vis system presented remarkably higher reaction rates with unadjusted and adjusted initial pH = 5.0, $k = 23 \pm 3$ L kJ^{-1} and $k = 23 \pm 4$ L kJ^{-1}, respectively. The speciation diagrams (Fig. S2c) present significantly higher fractions of Fe^{3+} chelated with Citrate in the pH range of interest, compared with Oxalate. However, after the very quick initial OTC decay, total antibiotic removal seems to be hindered by the competitive effect of the progressive formation of not only intermediary byproducts resulting from OTC oxidation, but also from intermediates resulting from the ferricitrate decarboxylation [22]. Feng et al. [44] reported good Tetracycline (0–40 1M) photodegradation results at near neutral pH values using Fe^{3+}-citrate with substantially higher iron/citrate molar ratios (from 1:10 up to 1:30). Nevertheless, this would imply a significant addition of extra dissolved carbon, in the order of dozens of mg C L^{-1}. As a result, no further experiments with the Fe^{3+}/ Citrate/H_2O_2/UV–Vis system were considered.

3.2.3. *Influence of temperature and irradiance*

When using photocatalytic systems under realistic conditions (solar pilot plants, for instance), special consideration must be given to two important process parameters, temperature and irradiance [45]. There is a natural variability in solar irradiance depending on time of day, season of the year, atmospheric conditions, and even latitude, while the process usually takes place at ambient temperature (thus also depending on some of the above- mentioned factors).

In this way, further Fe^{3+}/Oxalate/H_2O_2/UV–Vis experiments were performed under the chosen conditions (Section 3.2.2) to screen the effects of different temperature and irradiance values. Two typical water temperature values commonly achieved in summer and winter conditions in our CPC pilot-plant installation were tested, 12 and 35 ºC (Fig. 5a) and compared to the default set temperature (25 ºC). The lower reaction rate achieved with 12 ºC (3.4 ± 0.2 L kJ^{-1}) and the higher with 35 ºC (15.1 ± 0.6 L kJ^{-1}), while OTC was no longer quantifiable after 10 and 3 min of illumination time, respectively, reflect a positive role of temperature in the photo-Fenton process. The quantum yield of ferrioxalate is independent of temperature [46], but higher temperatures promote the regeneration rate of ferrous iron from ferric iron, thereby increasing hydroxyl radical production [11], which, in this case, seems to be analogous to a likely faster consumption of oxalic acid (there is a steeper reduction in the DOC content) reflected in the earlier and more accentuated decrease in total dissolved iron concentration. Higher temperatures were not tested, because they may promote an

inefficient H_2O_2 decomposition into H_2O and O_2 [47]. Lower irradiances, 24 and 37 W_{UV} m^{-2}, on the other hand, did not result in major differences compared to the default value (I = 44 W_{UV} m^{-2}), regarding the required illumination time to fully degrade OTC, nor in H_2O_2 consumption rates (Fig. 5b).

3.2.4. Influence of inorganic anions and humic acids

Keeping in mind the perspective of applying the proposed process to treat concentrated micropollutants in retentates originating from membrane processes operation, the retention of other constituents, which may affect the photo-Fenton process, also needs to be considered [48]. Inorganic anions, for instance, can concentrate up to the order of the hundreds of milligrams [25], and may affect the process by (i) complex formation with Fe^{2+} and Fe^{3+}, (ii) hydroxyl radicals scavenging and formation of less reactive inorganic radicals and (iii) oxidation reactions involving these inorganic radicals [49]. The presence of dissolved natural organic matter, such as humic acids (HA), may also hamper the process since it may bind the micropollutants themselves [50], attenuate incoming radiation [35], act as a hydroxyl radical sink and finally, although their binding with iron may increase its solubility, it alters its redox cycle and changes the formation rate of hydroxyl radicals [27].

For these reasons, a set of experiments was performed with 1 g L^{-1} of Cl^-, SO_4^{2-}, NO_3^-, 0.1 g L^{-1} of HCO_3^- and 5 mg C L^{-1} of HA to assess the individual effect of each interfering species in the degradation of OTC under the chosen conditions (Fig. 6). The required illumination time to bring the concentration of OTC under LOD levels only marginally increased in all experiments, except in the case of HA, which was longest. Likewise, HA was the only interfering species whose effect on the mineralization process was noteworthy, since initial DOC was only reduced by 35% against an average of 41% reduction compared to the other interfering species, and 46% in their absence, after 40 min of illumination time (Q_{UV} = 2.3 kJ L^{-1}). The overall consumption profiles of H_2O_2 reflected well these differences in mineralization degrees.

This apparent weak impact in the reaction efficiency in the presence of iron-complexing species such as Cl^-[4] or SO^{2-} could be also explained recurring to the study of the speciation of iron in solution. The equilibrium constants of ferrioxalate complexes are much higher than those of both Fe–Cl and Fe–SO_4 complexes [51], thus it can be seen in Fig. S2b (right) that, for instance, the introduction of 1 g L^{-1} of SO^{2-} when plotting the iron complexes in solution (with the respective ionic strength correction, 30 mM) only alters the distribution of the $Fe(C_2O_4)^-_2$ complex in favor of

$Fe(C_2O_4)^{3-}$, whereas none of the Fe–SO_4 complexes is shown to be formed at the pH range of interest.

3.2.5. Influence of the matrix

After assessing the potential influence of individual common wastewater components on the Fe^{3+}/Oxalate/H_2O_2/UV–Vis process, two different effluents were spiked with OTC (C_0 = 20 mg L^{-1}) to complementarily study the influence of real matrixes. Even though pH_0 = 5.0 was set beforehand as the chosen pH to study the process efficiency, experiments were also performed with pH_0 = 4.0 in each media. This was due to the fact that after the oxalate and Fe^{3+} addition steps, the pH of the trout farm (TF) effluent lowered to the same unadjusted pH of the deionized water (DW) solution, around 4.0. On the other hand, given composition of WW medium (Table 1), additional pH adjustment with acid was required, but it also helped to lower some of the initial inorganic carbon. The results comparing the efficiency of the process carried out in DW solution, WW and TF effluents are thus presented in Fig. 7. With pH_0 = 4.0, OTC was no longer detected after 10 min of illumination in WW effluent (Q_{UV}= 0.7 kJ L^{-1}), and after 6 min in TF effluent (Q_{UV} = 0.4 kJ L^{-1}). Required illumination times were higher in pH_0 = 5.0:20 min in WW effluent (Q_{UV} = 1.4 kJ L^{-1}), and 10 min in TF effluent (Q_{UV} = 0.7 kJ L^{-1}). The distribution of the ferric species in both media (Fig. S2c) seems to explain the similar kinetic degradation rates achieved with TF effluent, and the worse with WW (Table 2). At pH_0 = 4.0, some fraction of ferric ions in the form of the mineral Strengite ($FePO_4$ $2H_2O$ (s)) is already expected to be found in WW, while in TF medium results there is a relatively higher proportion of the more photo-active $Fe(C_2O_4)^{-}_2$ complex compared to that in DW (Fig. S2b). The proportion of $FePO_4$-$2H_2O$ (s) at pH_0 = 5.0 in both effluents clearly reflects the lower OTC kinetic degradation rates, especially in the case of WW effluent. Also to be considered is the abovementioned effect of the additional DOC/NOM content of both effluents in the overall process efficiency. Compared to the DW experiments, for instance, less H_2O_2 was consumed by the end of the photo-treatment period (45 min of illumination, Q_{UV} = 3.3 kJ L^{-1}), which may also reflect the lesser reduction in DOC content comparing with DW experiments at both tested pH values. Accounting for each effluent's initial DOC values, DOC reduction in WW effluent was of 39% and 31% for pH_0 = 4.0 and 5.0, respectively, whereas in TF effluent it was 56% and 49%, in the same order.

3.3. Solar pilot-plant experiment

An experiment was also carried out in the CPC pilot-plant (Fig. 8a) to compare the degradation of OTC by the Fe^{3+}/Oxalate/H_2O_2/UV–Vis system under real solar radiation conditions using the best conditions determined in the lab-scale experiments ($[Fe^{3+}] = 2$ mg L^{-1}, 1:3 iron/oxalate molar ratio, $pH_0 = 5.0$, total added $H_2O_2 = 90$ mg L^{-1} (3.1 mM)). To further increase the knowledge about the degradation efficiency, samples were also taken to follow-up the concentration of low molecular weight carboxylate anions (LMWCA, in terms of carbon content; individual concentrations in Fig. 8b) and to monitor the antibacterial activity of the treated solution against *E. coli* along the reaction. After the same amount of accumulated energy per litre of solution recorded in the lab-scale experiment ($Q_{UV} = 0.41$ kJ L^{-1}), OTC was no longer detected (Fig. 8a). At the same time, the remaining organic matter no longer exhibited antibacterial activity (Fig. S3). A similar behavior was reported in a previous work [31], where a solution containing 40 mg L^{-1} of OTC, treated with 0.5 g L^{-1} of TiO_2 in the same pilot-plant, lost its antibacterial activity against *E. coli* when OTC was nearly depleted after $Q_{UV} = 2.0$ kJ$_{UV}$ L^{-1}. Even though there was higher consumption of H_2O_2 along the same illumination period, the mineralization profile matches quite well with the one of the lab-scale experiment, achieving a final reduction of 51% of the initial DOC. The profile of the sum of LMWCA (plotted in mg C L^{-1}) can also be seen in Fig. 8a, where at $Q_{UV} = 0.0$ kJ$_{UV}$ L^{-1} only oxalate was present after the addition of the 3:1 M ratio to 2 mg L^{-1} of Fe^{3+} dose. After illumination started, and until $Q_{UV} = 0.41$ kJ$_{UV}$ L^{-1}, the period when OTC was mostly degraded, there was a quick conversion of DOC into carboxylic acids, as can be seen in Fig 8b. At this point, 61% of DOC consisted in still undepleted oxalate and in oxamate, tartronate, acetate, maleate and for- mate in smaller quantities. Afterwards, oxalic acid began to slowly deplete (corresponding well with the progressive decrease in the concentration of total dissolved iron), and until $Q_{UV} = 1.17$ kJ$_{UV}$ L^{-1} a peak of 72.5% of DOC in the form of LMWCA was achieved, equivalent to the point where the mineralization process began to slow down, achieving the abovementioned final DOC level, from which 67.2% is in the form of low concentrations of oxalate, oxamate, tartronate, acetate, malonate, maleate and formate anions. The hampering of the mineralization process along the illumination time parallels well with the decay of oxalate and the formation of the detected carboxylates. Some are generally quite stable in solution, such as acetate and formate [52], others are recalcitrant to hydroxyl radical attack [53], such as

oxamate, while others, though being able to form Fe^{3+}-complexes as well, have lower or non-existent quantum yields of Fe^{2+} formation, such as malonate [22]. Nevertheless, conversion of complex molecules into low- molecular weight molecules is associated with increases in biodegradability as a result of applying AOPs [54]. Regarding the fate of the nitrogen atoms present in the original 20 mg L^{-1} OTC solution (around 1.2 mg N L^{-1}), 60% of the original N content is in the detected oxamate by the end of the photo-treatment period. The remaining N content could not be quantified by the ion chromatography.

4. Conclusions

In this work, it was shown how the highly photo-active ferri- carboxylate complexes successfully promotes the photo-Fenton reaction in a lab-scale apparatus simulating solar radiation, equipped with a CPC photo-reactor, to remove the antibiotic Oxy- tetracycline from aqueous solution at near-neutral pH values. The oxalic acid in a 1:3 iron/oxalate molar ratio with the aim of forming iron/oxalate complexes showed to be better than citric acid in a 1:1 iron/citrate molar ratio in deterring the inconvenient formation of Fe:OTC complexes, which undermine OTC analytical detection and hamper the regeneration of Fe^{3+} into Fe^{2+}. Good antibiotic and DOC removals were achieved using the maximum allowed iron concentration in treated effluents (2 mg L^{-1} of Fe^{3+}), oxalic acid in a 1:3 iron/oxalate molar ratio, and the initial pH of 5.0, requiring overall low accumulated UV energy per liter of solution. Further- more, it was shown that these operating conditions are not remarkably affected by temperature, irradiance and presence of individual possible interfering species such as Cl^-, SO^{2-}, NO_3^- and HCO_3^-, while the presence of natural dissolved organic matter (humic acids) affected more the reaction. By contrast, experiments performed in a domestic WWTP effluent showed slower OTC removal kinetics and lower DOC reduction mainly due to the precipitation of $FePO_4(s)$. However, in a less complex effluent from the outlet of a trout farm it was shown that without the pH adjustment step, similar results were achieved, compared with deionized water experiments. An experiment carried out in a CPC pilot-plant under real solar radiation compared well with the lab-scale photo- reactor using simulated solar radiation. The treated solution loses antibacterial activity against *E. coli* as soon as OTC is degraded, and the remaining DOC is quickly converted to low-molecular- weight carboxylate anions. Although these are mostly recalcitrant to further mineralization by hydroxyl radical attack, they are easily biodegradable. Not only their final percentage in terms of DOC is quite high, but also, with the depletion of oxalic acid, the final pH achieved by the end of the treatment, also

meets the minimum discharge limit, reducing the need of relevant post-phototreatment steps.

Acknowledgements

This work was partially supported by projects PEst-C/EQB/ LA0020/2013, PTDC/AAC-AMB/113091/2009 and AQUAPHOTOBIO
– PP-IJUP-2011-180, financed by FEDER through COMPETE – Prog- rama Operacional Factores de Competitividade, by FCT – Fundação para a Ciência e a Tecnologia and U. Porto/Banco Santander Totta.
J.H.O.S. Pereira acknowledges his doctoral fellowship (SFRH/BD/ 62277/2009) supported by FCT – Fundação para a Ciência e a Tecnologia. V.J.P. Vilar acknowledges the FCT Investigator 2013 Programme (IF/01501/2013).

Appendix A. Supplementary data

Supplementary data associated with this article can be found, in the online version, at http://dx.doi.org/10.1016/j.cej.2014.05.037.

References

[1] K. Kümmerer, The presence of pharmaceuticals in the environment due to human use – present knowledge and future challenges, J. Environ. Manage. 90 (2009) 2354–2366.
[2] R. Loos, B.M. Gawlik, G. Locoro, E. Rimaviciute, S. Contini, G. Bidoglio, EU-wide survey of polar organic persistent pollutants in European river waters, Environ. Pollut. 157 (2009) 561–568.
[3] P. Verlicchi, A. Galletti, M. Petrovic, D. Barceló, Hospital effluents as a source of emerging pollutants: an overview of micropollutants and sustainable treatment options, J. Hydrol. 389 (2010) 416–428.
[4] M. Tamminen, A. Karkman, A. Lõhmus, W.I. Muziasari, H. Takasu, S. Wada, S. Suzuki, M. Virta, Tetracycline resistance genes persist at aquaculture farms in the absence of selection pressure, Environ. Sci. Technol. 45 (2011) 386–391.
[5] C.M. Manaia, I. Vaz-Moreira, O.C. Nunes, Antibiotic resistance in waste water and suface water and human health implications, in: D. Barceló (Ed.), Emerging Organic Contaminants and Human Health, Springer-Verlag Berling and Heidelberg GmbH & Co. KG, 2012, pp. 173–212.
[6] I. Michael, L. Rizzo, C.S. McArdell, C.M. Manaia, C. Merlin, T. Schwartz, C. Dagot, D. Fatta-Kassinos, Urban wastewater treatment plants as hotspots for the release of antibiotics in the environment: a review, Water Res. 47 (2013) 957–

995.
[7] G. Rigos, I. Nengas, M. Alexis, Oxytetracycline (OTC) uptake following bath treatment in gilthead sea bream (*Sparus aurata*), Aquaculture 261 (2006) 1151–1155.
[8] P.R. Gogate, A.B. Pandit, A review of imperative technologies for wastewater treatment II: hybrid methods, Adv. Environ. Res. 8 (2004) 553–597.
[9] V. Homem, L. Santos, Degradation and removal methods of antibiotics from aqueous matrices – A review, J. Environ. Manage. 92 (2011) 2304–2347.
[10] S. Malato, P. Fernández-Ibáñez, M.I. Maldonado, J. Blanco, W. Gernjak, Decontamination and disinfection of water by solar photocatalysis: recent overview and trends, Catal. Today 147 (2009) 1–59.
[11] J.J. Pignatello, E. Oliveros, A. MacKay, Advanced oxidation processes for organic contaminant destruction based on the fenton reaction and related chemistry, Crit. Rev. Environ. Sci. Technol. 36 (2006) 1–84.
[12] M.A. Ghandour, H.A. Azab, A. Hassan, A.M. Ali, Potentiometric studies on the complexes of tetracycline (TC) and oxytetracyclin (OTC) with some metal ions, Monatshefte für Chemie Chemical Monthly 123 (1992) 51–58.
[13] K.O. Ogunniran, A.C. Tella, M. Alensela, M.T. Yakubu, Synthesis, physical properties, antimicrobial potentials of some antibiotics complexed with transition metals and their effects on alkaline phosphatase activities of selected rat tissues, Afr. J. Biotechnol. 6 (2007) 1202–1208.
[14] P. Mikelens, W. Levinson, Nucleic-acid binding by tetracycline metal ion complexes, Bioinorg. Chem. 9 (1978) 421–429.
[15] W.D. Kong, Y.G. Zhu, B.J. Fu, P. Marschner, J.Z. He, The veterinary antibiotic oxytetracycline and Cu influence functional diversity of the soil microbial community, Environ. Pollut. 143 (2006) 129–137.
[16] A.D. Jones, G.L. Bruland, S.G. Agrawal, D. Vasudevan, Factors influencing the sorption of oxytetracycline to soils, Environ. Toxicol. Chem. 24 (2005) 761–770.
[17] B.A. Lalonde, W. Ernst, L. Greenwood, Measurement of oxytetracycline and emamectin benzoate in freshwater sediments downstream of land based aquaculture facilities in the Atlantic Region of Canada, Bull. Environ. Contam. Toxicol. 89 (2012) 547–550.
[18] A.P.S. Batista, R.F.P. Nogueira, Parameters affecting sulfonamide photo-Fenton degradation – iron complexation and substituent group, J. Photochem. Photobiol. A: Chem. 232 (2012) 8–13.
[19] C. Gu, K.G. Karthikeyan, Interaction of tetracycline with aluminum and iron hydrous oxides, Environ. Sci. Technol. 39 (2005) 2660–2667.
[20] J. Jeong, J. Yoon, PH effect on OH radical production in photo/ferrioxalate system, Water Res. 39 (2005) 2893–2900.
[21] W. Huang, M. Brigante, F. Wu, K. Hanna, G. Mailhot, Development of a new

homogenous photo-Fenton process using Fe(III)–EDDS complexes, J. Photochem. Photobiol. A: Chem. 239 (2012) 17–23.
[22] E.M. Rodríguez, B. Núñez, G. Fernández, F.J. Beltrán, Effects of some carboxylic acids on the Fe(III)/UVA photocatalytic oxidation of muconic acid in water, Appl. Catal. B 89 (2009) 214–222.
[23] M.R.A. Silva, A.G. Trovó, R.F.P. Nogueira, Degradation of the herbicide tebuthiuron using solar photo-Fenton process and ferric citrate complex at circumneutral pH, J. Photochem. Photobiol. A: Chem. 191 (2007) 187–192.
[24] P. Westerhoff, H. Moon, D. Minakata, J. Crittenden, Oxidation of organics in retentates from reverse osmosis wastewater reuse facilities, Water Res. 43 (2009) 3992–3998.
[25] S. Miralles-Cuevas, A. Arqués, M.I. Maldonado, J.A. Sánchez-Pérez, S. Malato Rodríguez, Combined nanofiltration and photo-Fenton treatment of water containing micropollutants, Chem. Eng. J. 224 (2013) 89–95.
[26] J.H.O.S. Pereira, A.C. Reis, O.C. Nunes, M.T. Borges, V.J.P. Vilar, R.A.R. Boaventura, Assessment of solar driven TiO2-assisted photocatalysis efficiency on amoxicillin degradation, Environ. Sci. Pollut. Res. (2013) 1–12.
[27] M.E. Lindsey, M.A. Tarr, Inhibition of hydroxyl radical reaction with aromatics by dissolved natural organic matter, Environ. Sci. Technol. 34 (2000) 444–449.
[28] N. Klamerth, L. Rizzo, S. Malato, M.I. Maldonado, A. Agüera, A.R. Fernández- Alba, Degradation of fifteen emerging contaminants at 1g L^{-1} initial concentrations by mild solar photo-Fenton in MWTP effluents, Water Res. 44 (2010) 545–554.
[29] J. Bacardit, I. Oller, M.I. Maldonado, E. Chamarro, S. Malato, S. Esplugas, Simple models for the control of photo-fenton by monitoring H2O2, J. Adv. Oxid. Technol. 10 (2007) 219–228.
[30] O. González, C. Sans, S. Esplugas, Sulfamethoxazole abatement by photo-Fenton. Toxicity, inhibition and biodegradability assessment of intermediates, J. Hazard. Mater. 146 (2007) 459–464.
[31] J.H.O.S. Pereira, A.C. Reis, D. Queirós, O.C. Nunes, M.T. Borges, V.P. Vilar, R.A.R. Boaventura, Insights into solar TiO2-assisted photocatalytic oxidation of two antibiotics employed in aquatic animal production, oxolinic acid and oxytetracycline, Sci. Total Environ. 463–464 (2013) 274–283.
[32] R.F.P. Nogueira, M.C. Oliveira, W.C. Paterlini, Simple and fast spectrophotometric determination of H2O2 in photo-Fenton reactions using metavanadate, Talanta 66 (2005) 86–91.
[33] J.H.O.S. Pereira, V.J.P. Vilar, M.T. Borges, O. González, S. Esplugas, R.A.R. Boaventura, Photocatalytic degradation of oxytetracycline using TiO2 under natural and simulated solar radiation, Sol. Energy 85 (2011) 2732–2740.

[34] Decreto-Lei no. 236/98 de 1 de Agosto 1998, in: Diário da República – I Série-A, Portugal, pp. 3676-3722. .
[35] I.R. Bautitz, R.F.P. Nogueira, Degradation of tetracycline by photo-Fenton process-Solar irradiation and matrix effects, J. Photochem. Photobiol. A: Chem. 187 (2007) 33–39.
[36] R.A. Figueroa, A.A. Mackay, Sorption of oxytetracycline to iron oxides and iron oxide-rich soils, Environ. Sci. Technol. 39 (2005) 6664–6671.
[37] A. Albert, Avidity of terramycin and aureomycin for metallic cations, Nature 172 (1953) 201.
[38] W.D. Schecher, D.C. McAvoy, MINEQL+: a chemical equilibrium modeling system, version 4.5 for windows workbook, Environmental Research Software, 2003.
[39] D. Zhou, J. Wang, L. Hou, J. Xu, Y. Zhao, Photochemistry of Fe(III)-tetracycline complexes in aqueous solution under UV irradiation, in: Guilin, Guangxi, 2012, pp. 608–611.
[40] M.R.A. Silva, W. Vilegas, M.V.B. Zanoni, R.F. Pupo Nogueira, Photo-Fenton degradation of the herbicide tebuthiuron under solar irradiation: iron complexation and initial intermediates, Water Res. 44 (2010) 3745–3753.
[41] C. Weller, S. Horn, H. Herrmann, Effects of Fe(III)-concentration, speciation, excitation-wavelength and light intensity on the quantum yield of iron(III)- oxalato complex photolysis, J. Photochem. Photobiol. A: Chem. 255 (2013) 41–49.
[42] M.E. Balmer, B. Sulzberger, Atrazine degradation in irradiated iron/oxalate systems: effects of pH and oxalate, Environ. Sci. Technol. 33 (1999) 2418–2424.
[43] C. Zhao, M. Pelaez, X. Duan, H. Deng, K. O'Shea, D. Fatta-Kassinos, D.D. Dionysiou, Role of pH on photolytic and photocatalytic degradation of antibiotic oxytetracycline in aqueous solution under visible/solar light: kinetics and mechanism studies, Appl. Catal. B 134–135 (2013) 83–92.
[44] X. Feng, Z. Wang, Y. Chen, T. Tao, F. Wu, Multivariate-parameter optimization for photodegradation of tetracycline by Fe(III)–citrate complexes at near- neutral pH, J. Environ. Eng. 138 (2012) 873–879.
[45] A. Zapata, I. Oller, E. Bizani, J.A. Sánchez-Pérez, M.I. Maldonado, S. Malato, Evaluation of operational parameters involved in solar photo-Fenton degradation of a commercial pesticide mixture, Catal. Today 144 (2009) 94–99.
[46] D.E. Nicodem, O.M.V. Aquilera, Standardization of the potassium ferrioxalate actinometer over the temperature range 5–80 ºC, J. Photochem. 21 (1983) 189–193.
[47] J.M. Monteagudo, A. Durán, R. Culebradas, I. San Martín, A. Carnicer, Optimization of pharmaceutical wastewater treatment by solar/ferrioxalate photo-catalysis, J. Environ. Manage. 128 (2013) 210–219.

[48] F. Martínez, M.J. López-Muñoz, J. Aguado, J.A. Melero, J. Arsuaga, A. Sotto, R. Molina, Y. Segura, M.I. Pariente, A. Revilla, L. Cerro, G. Carenas, Coupling membrane separation and photocatalytic oxidation processes for the degradation of pharmaceutical pollutants, Water Res. 47 (2013) 5647–5658.
[49] J. De Laat, G. Truong Le, B. Legube, A comparative study of the effects of chloride, sulfate and nitrate ions on the rates of decomposition of H2O2 and organic compounds by Fe(II)/H2O2 and Fe(III)/H2O2, Chemosphere 55 (2004) 715–723.
[50] C. Gu, K.G. Karthikeyan, S.D. Sibley, J.A. Pedersen, Complexation of the antibiotic tetracycline with humic acid, Chemosphere 66 (2007) 1494–1501.
[51] G.L. Truong, J.D. Laat, B. Legube, Effects of chloride and sulfate on the rate of oxidation of ferrous ion by H2O2, Water Res. 38 (2004) 2384–2394.
[52] M.I. Franch, J.A. Ayllón, J. Peral, X. Domènech, Fe(III) photocatalyzed degradation of low chain carboxylic acids: implications of the iron salt, Appl. Catal. B 50 (2004) 89–99.
[53] S. Garcia-Segura, E. Brillas, Mineralization of the recalcitrant oxalic and oxamic acids by electrochemical advanced oxidation processes using a boron-doped diamond anode, Water Res. 45 (2011) 2975–2984.
[54] L. Bijan, M. Mohseni, Integrated ozone and biotreatment of pulp mill effluent and changes in biodegradability and molecular weight distribution of organic compounds, Water Res. 39 (2005) 3763–3772.

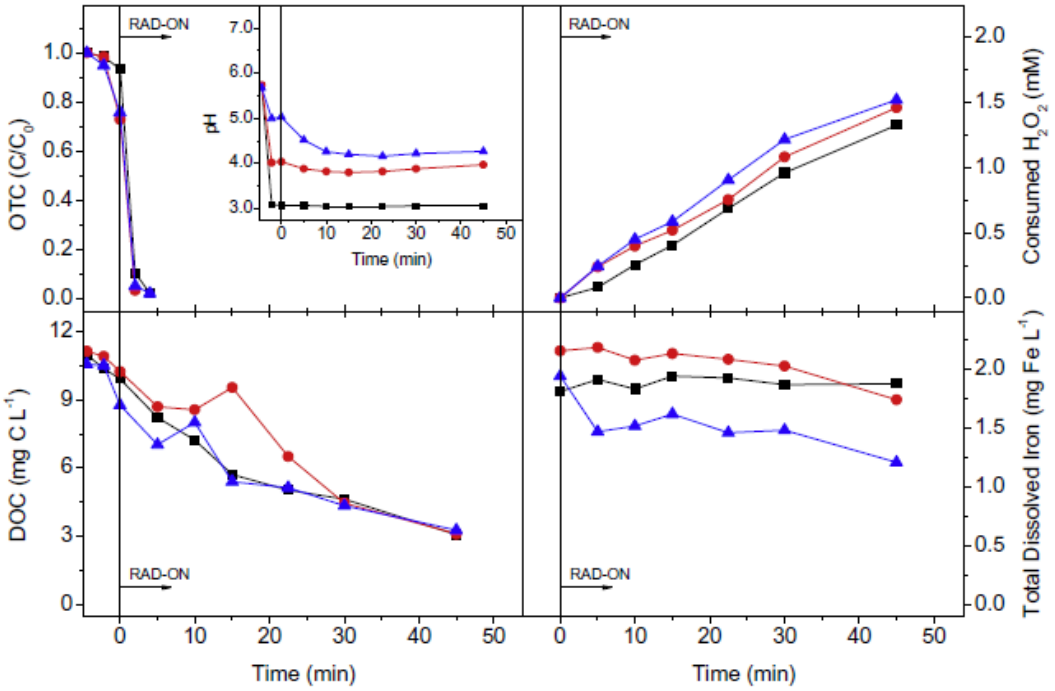

Fig. 1. Effect of initial pH (■ – pH = 3.0; ● – pH = 4.0; ▲ – pH = 5.0) on the degradation of OTC (C_0 = 20 mg L^{-1}) using conventional solar photo-Fenton process mediated by 2 mg L^{-1} Fe^{2+} in the lab-scale photoreactor. Follow-up of OTC degradation, DOC removal, H_2O_2 consumption, total dissolved iron and pH. Process parameters: T = 25 °C, I = 44 W_{UV} m^{-2}, total added H_2O_2 = 90 mg L^{-1}.

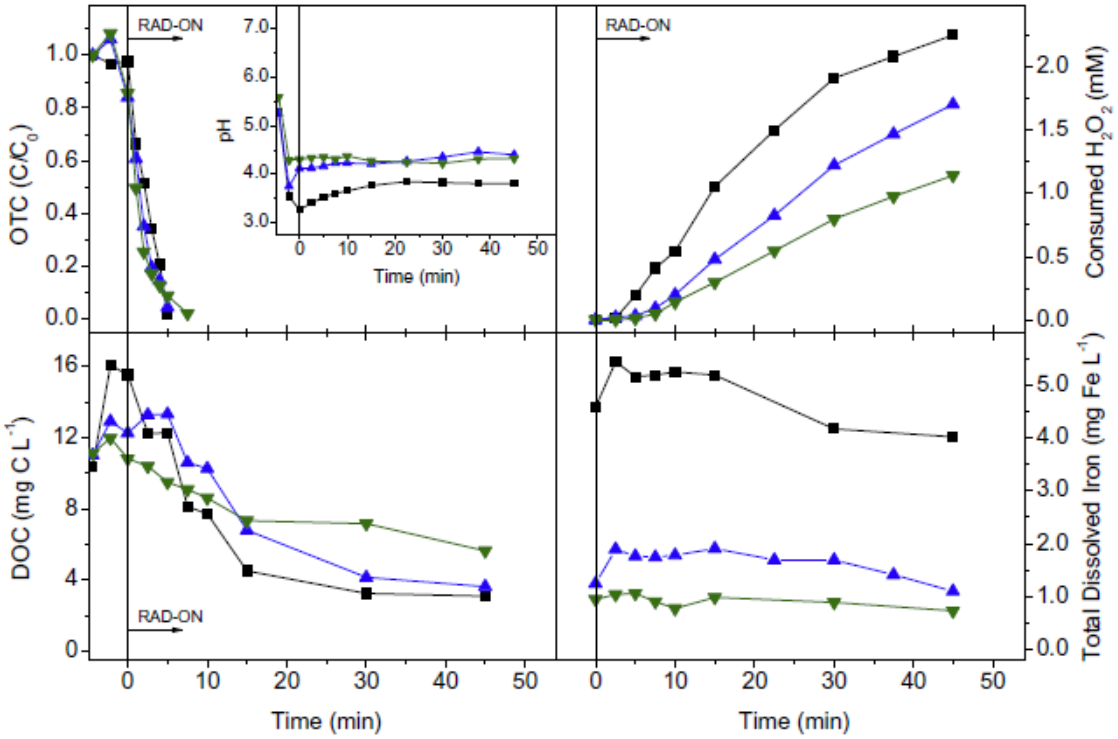

Fig. 2. Effect of Fe^{3+} concentration (▼ – 1.0 mg L^{-1}; ▲ – 2.0 mg L^{-1}; ■ – 5.0 mg L^{-1}) on the degradation of OTC (C_0 = 20 mg L^{-1}) using solar photo-Fenton process mediated by ferrioxalate (1:3 iron/oxalate molar ratio) in the lab-scale photoreactor. Follow-up of OTC degradation, DOC removal, H_2O_2 consumption, total dissolved iron and pH. Process parameters: T = 25 °C, I = 44 W_{UV} m^{-2}, initial pH unadjusted and total added H_2O_2 = 3.1 mM.

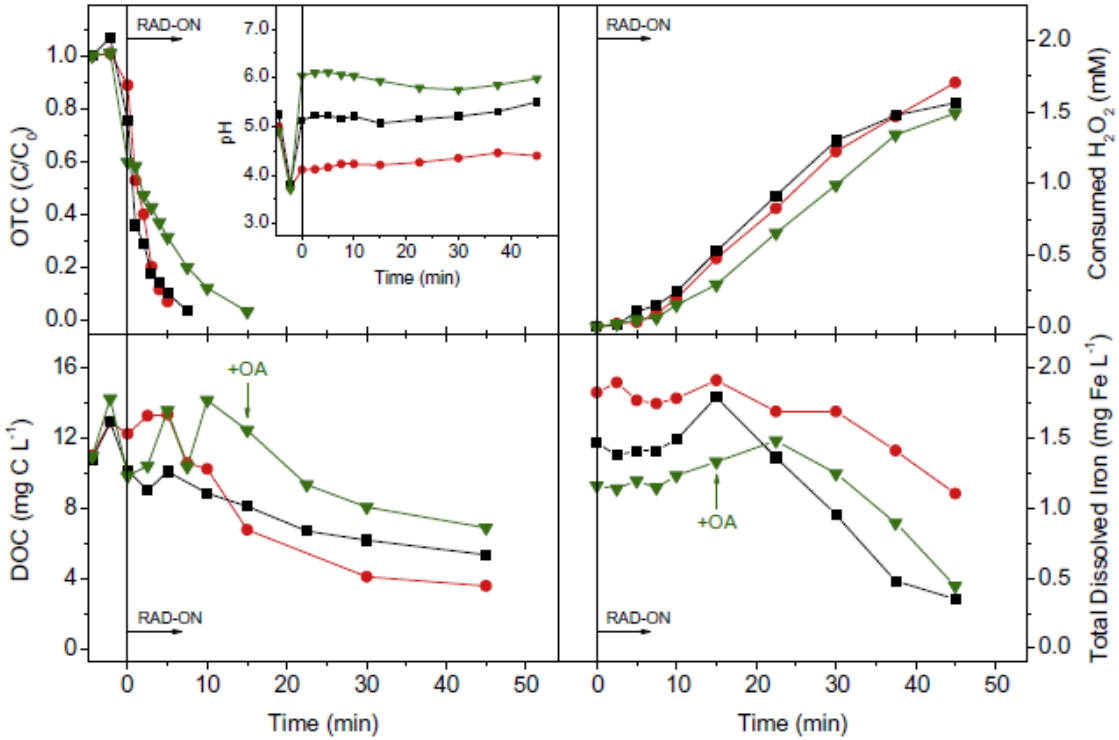

Fig. 3. Effect of initial pH (● – $pH_0 \sim 4.0$; ■ – $pH_0 = 5.0$; ▼ – $pH_0 = 6.0$) on the degradation of OTC ($C_0 = 20$ mg L^{-1}) using solar photo-Fenton process mediated by 2 mg L^{-1} Fe^{3+} and a 1:3 iron/oxalate molar ratio in the lab-scale photoreactor. Follow-up of OTC degradation, DOC removal, H_2O_2 consumption, total dissolved iron and pH. Process parameters: $T = 25$ °C, $I = 44$ W_{UV} m^{-2} and total added $H_2O_2 = 3.1$ mM.

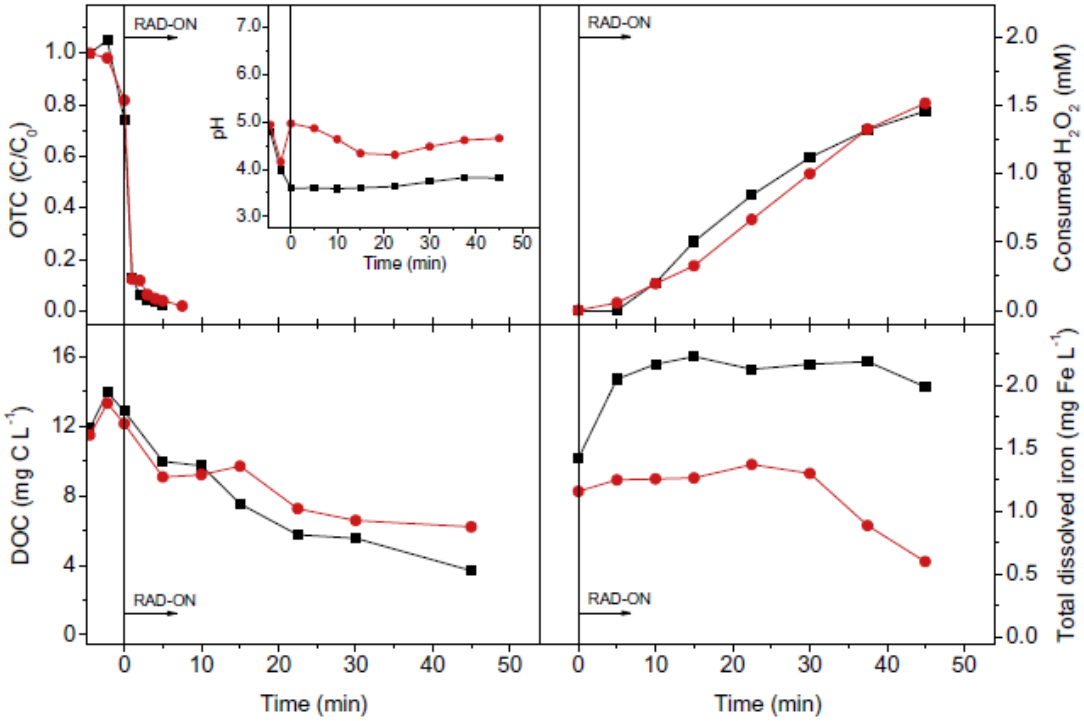

Fig. 4. Effect of initial pH (■ – $pH_0 \sim 3.6$, ● – $pH_0 = 5.0$) on the degradation of OTC ($C_0 = 20$ mg L^{-1}) using solar photo-Fenton process mediated by 2 mg L^{-1} Fe^{3+} and a 1:1 iron/citrate molar ratio in the lab-scale photoreactor. Follow-up of OTC degradation, DOC removal, H_2O_2 consumption, total dissolved iron and pH. Process parameters: $T = 25$ °C, $I = 44$ W_{UV} m^{-2} and total added $H_2O_2 = 3.1$ mM.

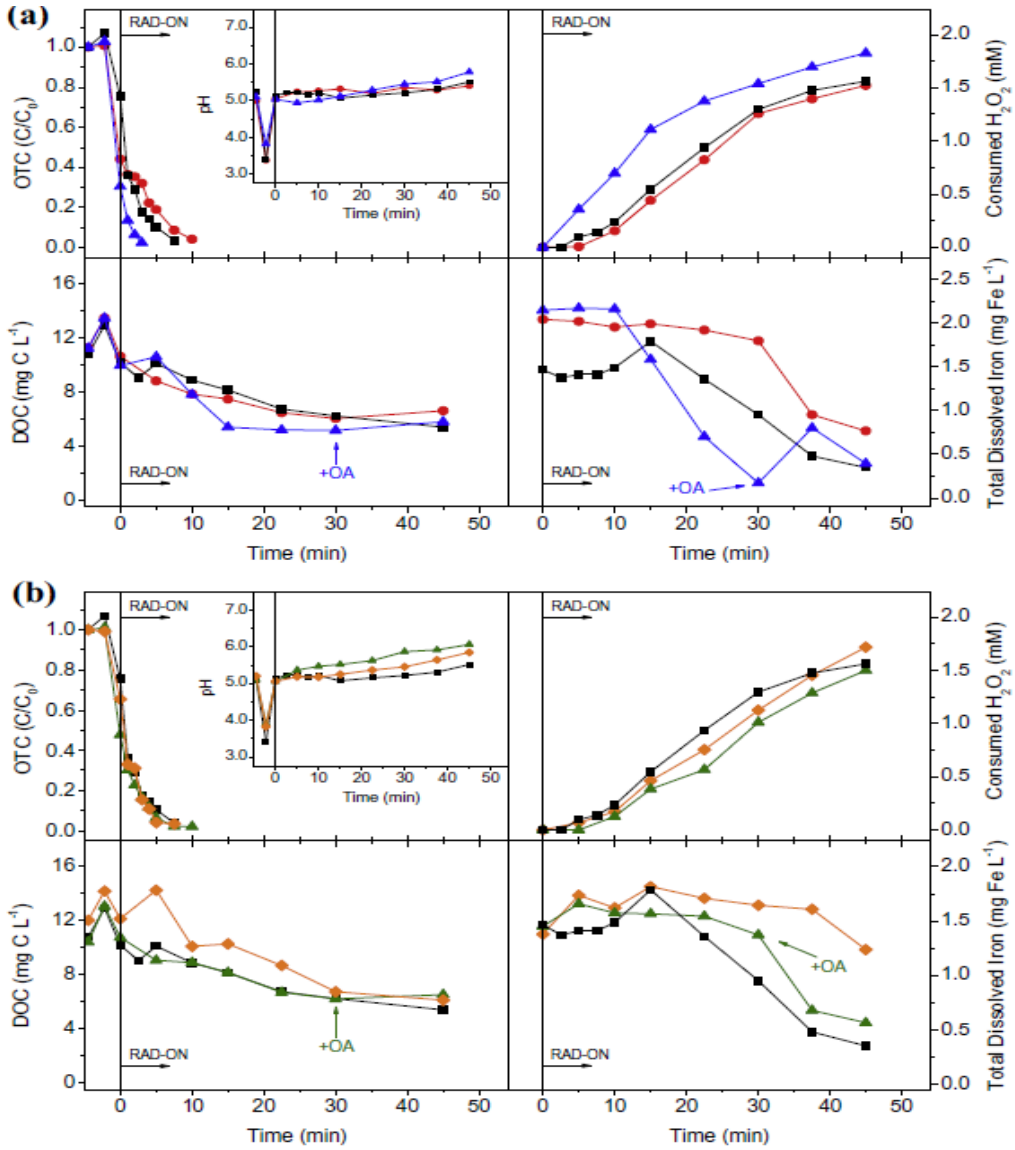

Fig. 5. Degradation of OTC (C_0 = 20 mg L^{-1}) using solar photo-Fenton process mediated by 2 mg L^{-1} Fe^{3+} and a 1:3 iron/oxalate molar ratio in the lab-scale photoreactor. Follow-up of OTC degradation, DOC removal, H_2O_2 consumption, total dissolved iron and pH. Process parameters: pH_0 = 5.0 and total added H_2O_2 = 3.1 mM. Effect of: (a) Initial temperature (● – T = 12 °C; ■ – T = 25 °C; ▲ – T = 35 °C), I = 44 W_{UV} m^{-2}; (b) Radiation intensity (◆ – I = 24.7 W_{UV} m^{-2}; ▲ – I = 37 W_{UV} m^{-2}; ■ – I = 44 W_{UV} m^{-2}), T = 25 °C.

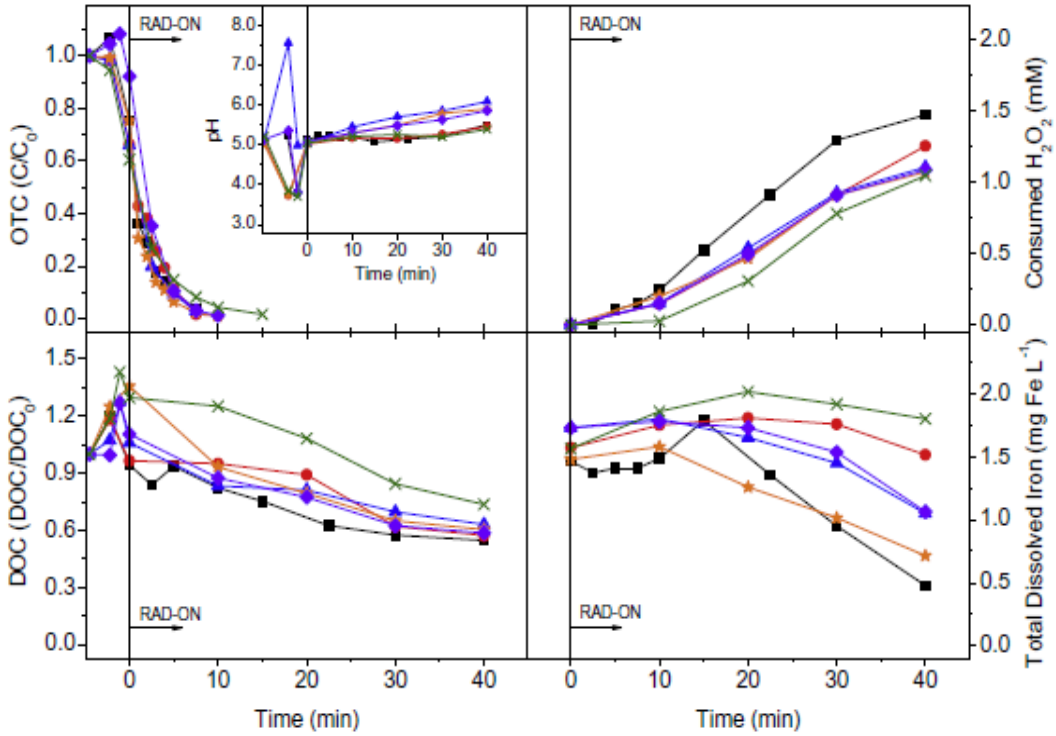

Fig. 6. Follow-up of OTC degradation (C_0 = 20 mg L^{-1}), DOC removal, H_2O_2 consumption, total dissolved iron and pH in the absence (■) and in the presence of 1 g L^{-1} of Cl^- (●), SO_4^{2-} (★), NO_3^- (♦), 0.1 g L^{-1} of HCO_3^- (▲), 5 mg C L^{-1} of HA (×) using the solar photo-Fenton process mediated by 2 mg L^{-1} Fe^{3+} and a 1:3 iron/oxalate molar ratio in the lab-scale photoreactor. Process parameters: pH_0 = 5.0, T = 25 °C, I = 44 W_{UV} m^{-2} and total added H_2O_2 = 3.1 mM.

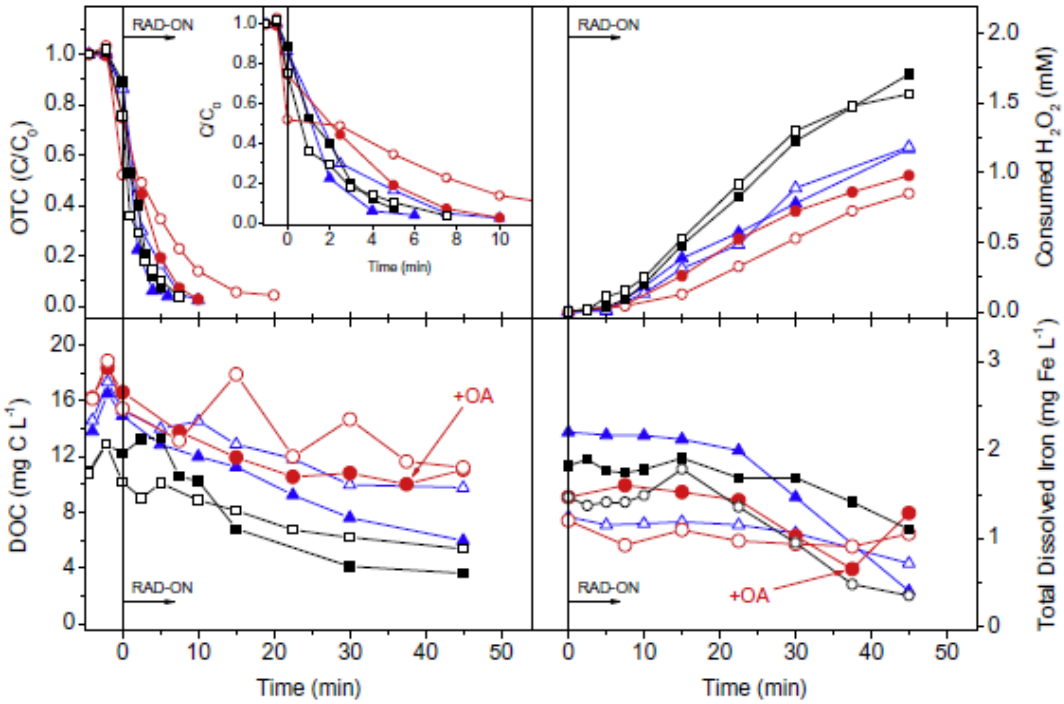

Fig. 7. Effect of the matrix on OTC degradation (C_0 = 20 mg L^{-1}), DOC removal, H_2O_2 consumption and total dissolved iron using the solar photo-Fenton process mediated by 2 mg L^{-1} Fe^{3+} and a 1:3 iron/oxalate molar ratio, performed at pH_0 = 4.0 (closed symbols) and pH_0 = 5.0 (open symbols), in the lab-scale photoreactor. Matrixes: DW (■, □), TF (▲, △) WW (●, ○). Process parameters: T = 25 °C, I = 44 W_{UV} m^{-2} and total added H_2O_2 = 3.1 mM.

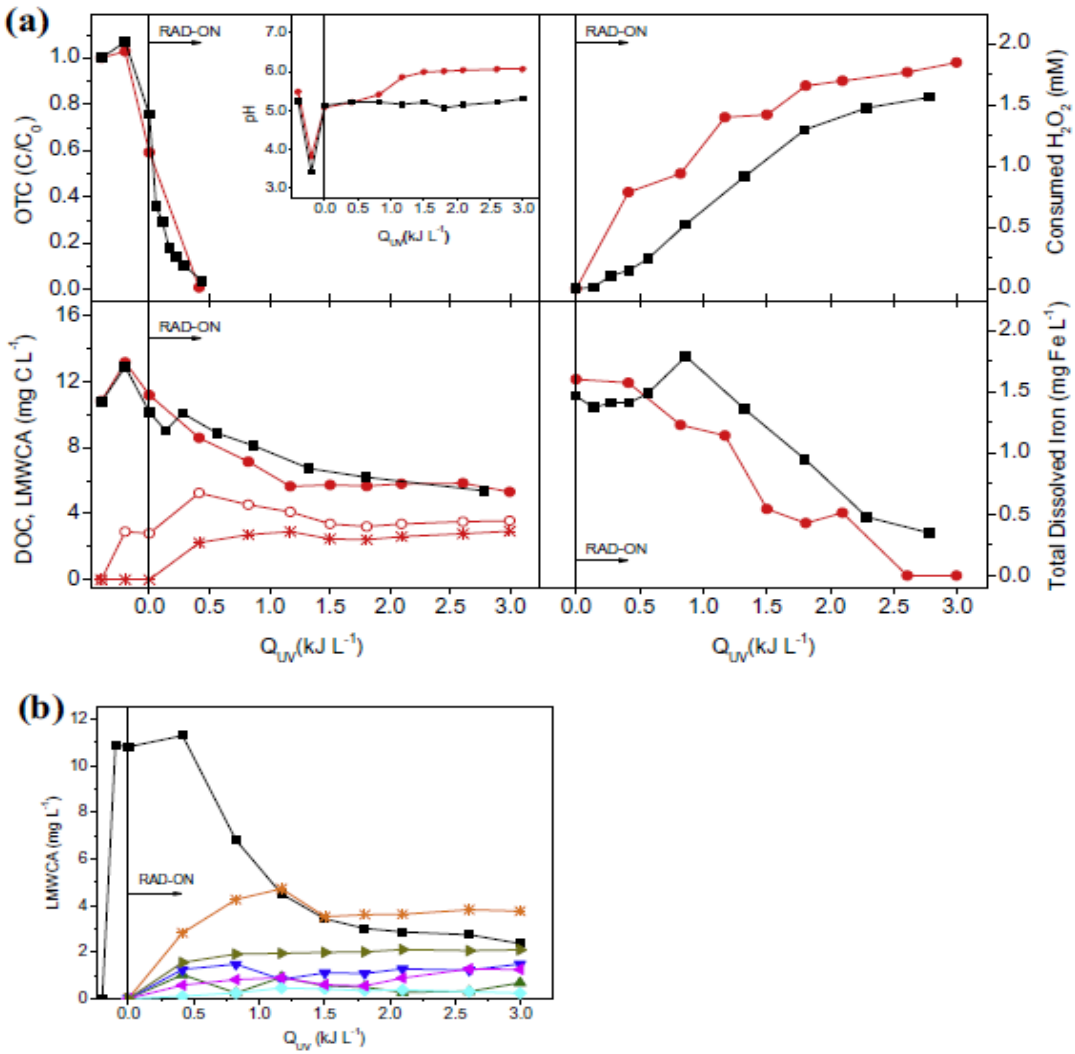

Fig. 8. (a) Evolution profiles of OTC degradation (C_0 = 20 mg L^{-1}), DOC removal, H_2O_2 consumption, total dissolved iron and pH using the solar photo-Fenton process mediated by 2 mg L^{-1} Fe^{3+} and a 1:3 iron/oxalate molar ratio, performed in the lab-scale photoreactor (■) and in the pilot-plant (●). (b) The sum of LMWCA in the pilot-plant experiment is shown with (○) and without (✳) initial oxalate concentration. Common process parameters: pH_0 = 5.0 and total added H_2O_2=3.1 mM. Lab-scale experiment process parameters: T = 25 °C, I = 44 W_{UV} m^{-2}; pilot-plant average process parameters: $\bar{T} = 26^{\circ}C, \bar{UV}_G = 16 W_{UV} m^{-2}$.

Table 1
Main characteristics of the tested effluents, before the OTC-spike step

Effluente	pH	DOC/IC	Average anion concentrations ($mg\ L^{-1}$)		
		($mg\ L^{-1}$)	$[PO_4^{3-}]$	$[Cl^-]$	$[SO_4^{2-}]$
WW	6.46	5.5/5.1	13.5	61.5	42.9
TF	6.70	3.9/1.8	0.95		

Table 2

Pseudo-first-order kinetic parameters for the Fe^{3+}/Oxalate/H2O2/UV–Vis process on the degradation of OTC (C0 = 20 mg L^{-1}). Iron/oxalate molar ratio: 1:3. Overall conditions: total added H2O2 = 3.1 mM; T = 25 ºC; I = 44 WUV m^{-2}.

Experiment		k (L kJ^{-1})[a]	R^2	S_R^2 (mg^2 L^{-2})
Influence of iron concentration (unadjusted pH)				
$[Fe^{3+}]$ = 1 mg L^{-1}		7.6 ± 0.4	0.993	0.207
$[Fe^{3+}]$ = 2 mg L^{-1}		8.6 ± 0.5	0.988	2.111
$[Fe^{3+}]$ = 5 mg L^{-1}		15.8 ± 0.8	0.994	1.076
Influence of initial pH ($[Fe^{3+}]$ = 2 mg L^{-1})				
$pH_0 \sim 4.0$		8.6 ± 0.5	0.988	2.111
pH_0 = 5.0		6.3 ± 0.2	0.990	0.065
pH_0 = 6.0		2.3 ± 0.1	0.990	0.146
Influence of temperature and irradiance ($[Fe^{3+}]$ = 2 mg L^{-1}, pH_0 = 5.0)				
T = 12 °C		3.4 ± 0.2	0.989	0.107
T = 35 °C		15.1 ± 0.6	0.998	0.012
I = 37 W_{UV} m^{-2}		7.5 ± 0.4	0.994	0.111
I = 24 W_{UV} m^{-2}		18 ± 2	0.987	0.513
Influence of inorganic ions and humic acids ($[Fe^{3+}]$ = 2 mg L^{-1}, pH_0 = 5.0)				
+1.0 g L^{-1} Cl^-		5.8 ± 0.4	0.971	0.823
+1.0 g L^{-1} SO_4^{2-}		9.3 ± 0.9	0.974	0.541
+0.1 g L^{-1} HCO_3^-		7.9 ± 0.5	0.997	0.126
+1.0 g L^{-1} NO_3^-		7.2 ± 0.3	0.999	0.083
+5.0 mg C L^{-1} HA		5.3 ± 0.2	0.998	0.066
Influence of the matrix ($[Fe^{3+}]$ = 2 mg L^{-1})				
WW effluent	pH_0 = 4.0	3.7 ± 0.3	0.991	0.417
	pH_0 = 5.0	1.5 ± 0.2	0.964	0.799
TF effluent	pH_0 = 4.0	9.59 ± 0.04	0.999	0.001
	pH_0 = 5.0	5.6 ± 0.4	0.997	0.277

[a] Pseudo-first order kinetic rate.